RSC Advances

ROYAL SOCIETY OF CHEMISTRY

www.rsc.org/advances

Journal Name

ARTICLE

Ultrafine Porous Boron Nitride Nanofibers Synthesized via Freeze-drying and Pyrolysis Process and Their Adsorption Properties

Received 00th January 20xx,
Accepted 00th January 20xx

DOI: 10.1039/x0xx00000x

www.rsc.org/

Jing Lin,[a,b] Lulu Xu,[a] Yang Huang,[a,*] Jie Li,[a] Weijia Wang,[a] Congcong Feng,[a] Zhenya Liu,[a] Xuewen Xu,[a] Jin Zou,[b,c] and Chengchun Tang[a,*]

One-dimensional (1D) boron nitride (BN) nanostructures with high aspect ratio are of prime interest due to their importance in fundamental research and wide-range potential applications. Herein we developed a facile method for the first synthesis of ultrafine porous BN nanofibers in a high purity and high yield. The method included two-steps, freeze-drying of hot melamine/boric acid solution and post pyrolysis of the as-obtained products. The extremely rapid cooling of hot melamine/boric acid solution during freeze-drying process resulted in the formation of ultrafine precursors, which was the key for final synthesis of porous BN nanofibers with downsized diameters (20-60 nm) and high aspect ratios. The as-synthesized ultrafine BN nanofibers possessed a high specific surface area and a large pore volume, which could be tuned by the pyrolysis parameters. All of these characteristics make the porous BN nanofibers promising in the application of water treatment, hydrogen storage, catalyst support, etc. Especially, an ultrafast adsorption of methylene blue (MB) in water has been demonstrated using the present porous BN nanofibers as adsorbent.

Introduction

One-dimensional (1D) nanostructures such as nanowires, nanotubes, nanofibers, have attracted much attention due to their wide-range potential applications and fundamental interests.[1-4] Hexagonal boron nitride (hBN), with a structural analogue of graphite, is an important ceramic material with high thermal conductivity, electrical insulation, superb oxidation resistance and chemical inertness.[5-6] 1D BN nanostructure is a promising nanomaterial in many application fields, such as functional composites, hydrogen storage, etc. BN nanotubes (BNNTs) have been considered as the most widely studied 1D BN nanostructures.[7-12] However, the practical application of BNNTs has been hindered due to the difficulties existing in BNNT synthesis with well-controlled morphology, high purity, large quantity and low costs.[5, 7-8] 1D porous BN nanofibers may be an alternative candidate as the substitution of BNNTs in many applications such as nanofillers in functional composites and building blocks in filtration membranes due to their high aspect ratios and porous structure. Superior to BNNTs, porous BN usually has much higher specific surface area, larger pore volume, lower density and plenty more active reaction sites, [13-15] thus displays superior performance as adsorbents for wastewater treatment, hydrogen storage, and catalyst carriers, etc.[16-25] However, compared with BNNTs, the development of high quality 1D porous BN nanostructures have been paid less attention.

In recent years, BN in porous structures have been synthesized in many methods, i.e. replica fabrication using templates, elemental substitution, etc.[13-17, 19-23] However, the controlled synthesis of porous BN in 1D nanostructures has been seldom achieved. G. Lian et al prepared BN ultrathin nanofiber network and hollow nanorods via a solvothermal process using NH_4BF_4 and NaN_3 as source materials.[18, 26] The porous BN nanostructures presented promising adsorption and hydrogen uptake property. However, their harsh reaction conditions and using of toxic precursors will be a great concern when scale up. It is highly desired to develop a green and low-cost method to obtain 1D porous BN nanostructures with well-controlled morphology, high aspect ratios, high purity and large quantities.

In this paper, we report a green two-step method for the first synthesis of 1D porous BN nanostructures in a high yield. The product consists of novel ultrafine 1D nanofibers with high porosity, which is quite distinct from the well-known BN nanotubes. Readily available and inexpensive boric acid and melamine was used as the starting materials. A freeze-drying process has been designed to successfully downsize the melamine diborate ($C_3N_6H_6{\cdot}2H_3BO_3$, M·2B) precursor into ultrafine 1D nanostructures. After a high-temperature

[a] School of Materials Science and Engineering, Hebei University of Technology, Tianjin 300130, P.R. China. E-mail: huangyang@hebut.edu.cn (Y. H.); tangcc@hebut.edu.cn (C. T.)
[b] Materials Engineering, The University of Queensland, St Lucia, QLD 4072, Australia.
[c] Centre for Microscopy and Microanalysis, The University of Queensland, St Lucia, QLD 4072, Australia.

†Electronic Supplementary Information (ESI) available: SEM image of the M·2B precursor, SEM image of M·2B whiskers synthesized via a naturally cooling process, TEM images of porous BN whiskers, isotherm parameters for the adsorption of MB on porous BN nanofibers, and adsorption test of Rhodamine B using porous BN nanofibers.

pyrolysis process, porous BN nanofibers with diameters of 20-60 nm can be obtained in a high yield and high purity. Especially, a rapid adsorption rate of the present nanofibers for methylene blue (MB) removal in water indicates a prospect for utilization of the present porous BN nanofibers for water treatment.

Experimental

Synthesis. In a typical synthesis, 4.64 g of H_3BO_3 and 3.15 g of $C_3N_6H_6$ were dissolved in 250 ml of distilled water. The reaction mixtures were heated at 85 °C for 4 h. Then the hot aqueous solution was frozen by liquid nitrogen and dried using a vacuum freeze dryer for 2-3 days to get the white precursor, i.e. M·2B ($C_3N_6H_6 \cdot 2H_3BO_3$) nanofibers. Then the white precursor was transferred to a tube furnace and heated to 1000-1300°C for 4 h to perform the pyrolysis treatments. All reactions were carried out in a flow of N_2 (0.5 L/min). After the synthesis, the system was cooled to room temperature. Finally a white wool-like product was obtained.

Adsorption tests. MB ($C_{16}H_{18}N_3SCl$) was dissolved in deionized water and then diluted to the required concentration before use. Then the porous BN nanofibers were added into the MB solution and UV-Vis absorption spectra were recorded at different time intervals. The adsorption tests were carried out with different initial concentrations to obtain the isotherms. The dye removal percentage over the adsorbent was calculated by $\eta\ (\%)=(C_0-C_e)\cdot 100/C_0$, where C_0 and C_e (mg/L) are the initial solution concentration and equilibrium concentration, respectively, and η is the pollutant removal percentage of the pollutants. The adsorption isotherms are fitted by the Langmuir adsorption model $q_e=q_mKC_e/(1+KC_e)$, where q_e is the adsorbed amount of pollutant on the equilibrium concentration (mg/g), C_e is the equilibrium concentration in solution (mg/L), q_m is the maximum adsorption capacity corresponding to complete monolayer covering on the adsorbents (mg/g), and K is the equilibrium constant related to the free energy of adsorption (L/mg).

Materials characterization. The morphology and structure of the products were studied using X-ray powder diffraction (XRD, BRUKER D8 FOCUS), field emission scanning electron microscopy (SEM, HITACHI S-4800), and 200 kV high-resolution transmission electron microscope (HRTEM, Philips Tecnai F20) equipped with an electron energy loss spectrometer (EELS). The nitrogen physisorption isotherms were measured at 77 K on an AutoSorb iQ-C TCD analyzer. Prior to the measurement, the samples were activated in vacuum at 300 °C for 8 h. The Brunauer-Emmett-Teller (BET) specific surface area was calculated from the nitrogen adsorption data in the relative pressure ranging from 0.07 to 0.2. Due to the broad pore size distribution ranging from micropores to mesopores, the Non-Local density functional theory (NLDFT) method was used to calculate the pore widths and pore size distributions (ASiQwin software). A double beam UV/Vis spectrophotometer (HITACHI, U-3900H) was used to determine the concentration of MB samples.

Results and Discussion

The controlled synthesis of ultrafine BN nanofibers was realized via a template-free method using melamine and boric acid as source materials. The experimental scheme is shown in Fig. 1. Firstly, the hot melamine/boric acid solution was frozen by liquid nitrogen. Then the precursor - melamine diborate nanofibers - were prepared via a subsequently drying process. After a high-temperature pyrolysis treatment, ultrafine BN nanofibers were obtained. The extremely rapid cooling process played an important role for the formation of ultrafine BN nanofibers, while the micro-structure of the BN nanofibers could be tuned by the pyrolysis parameters (will be discussed later).

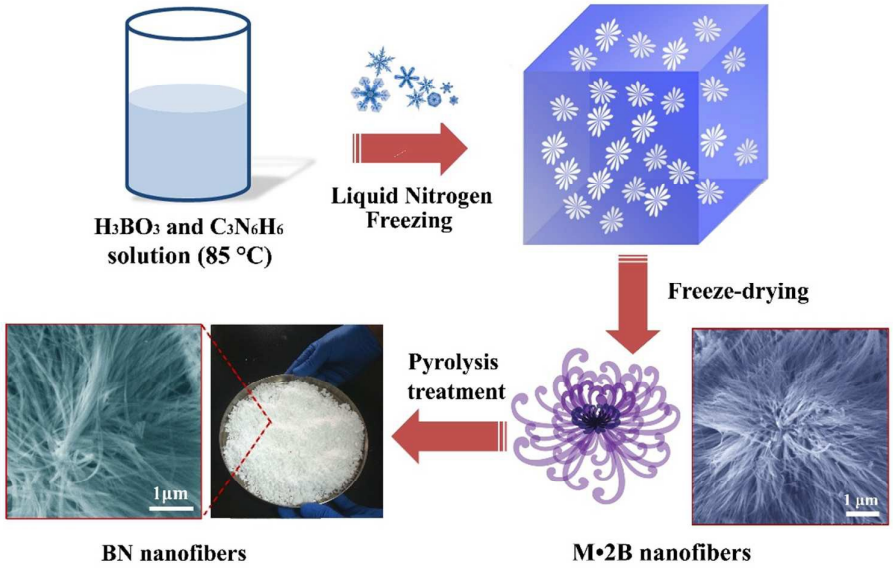

Fig. 1. Experimental scheme of the freeze-drying and pyrolysis synthesis of porous BN nanofibers.

The final product obtained after a single experimental run is shown in Fig. 2a, indicating a large-scale production. Fig. 2b is a typical SEM image of the as-prepared product (pyrolysis treated at 1100 °C), displaying 1D nanofibers with high purity. The length of the nanofibers varies from several to tens of micrometers. The SEM images verify that the pyrolysis treated product remains similar morphology as the M·2B precursor, as shown in Fig. S1 (Supporting Information). A typical low-magnification TEM image (Fig. 2c) indicates that the nanofibers are very flexible and display high aspect ratios. Enlarged TEM image (Fig. 2d) shows nanofibers with diameters less than 100 nm usually crystallize as bundles. All of the nanofibers exhibit a high porosity structure, which is quite different from the normally reported BN nanotubes with smooth surfaces.

Detailed TEM analysis further reveals the porous nature of the nanofibers. Fig. 3a and 3b show a bright-field STEM image and the corresponding high-angular dark-field (HAADF) STEM image of the nanofibers, respectively. It is known that the contrast of HAADF image is strongly dependent on the average atomic number of atoms in the sample. In Fig. 3b, the nanofibers display as bright nanowires with randomly distributed dark points, which represent the micropores in the nanofibers. Fig. 3c-d depict representative TEM images of individual nanofibers, respectively. All of the nanofibers have randomly distributed pores and nanofibers with diameters of 20-60 nm have most frequently been observed. Fig. 3d shows a single nanofiber with downsized diameter of sub-10 nm. High resolution TEM image (Fig. 3e) clearly reveals that the nanofiber has disordered BN layers. The crystallized BN layers interlink and form many disordered cavities inside the nanofiber (marked by the arrows). The corresponding SAED pattern (shown inset of Fig. 3e) further indicates the polycrystalline characteristic of the BN nanofiber.

Fig. 4a-d show HRTEM images of BN nanofibers prepared at different pyrolysis temperatures (from 1000 to 1300°C), respectively. The BN nanofibers obtained at 1000°C contain both amorphous and crystalline phases (Fig. 4a). With an increase of the pyrolysis temperature, the crystalline phases gradually become dominant (Fig. 4b-4d). In fact, a higher temperature is favourable for the growth of crystalline BN with ordered layers.[21] This phenomenon can be confirmed by XRD investigation, as shown in Fig. 4e, in which gradually increased (0002) peaks are observed for the different products. It is noted that the (0002) peaks are located at 2θ=24.2-25.4°, indicating an average lattice distance of 0.376-0.359 nm. These d_{0002} values are much larger than that in the BN nanotubes and bulk hexagonal-BN, revealing a turbostratic BN phase of the porous nanofibers. Besides, with increasing the pyrolysis temperature, a slight shift of the (0002) peaks toward to larger 2θ can be

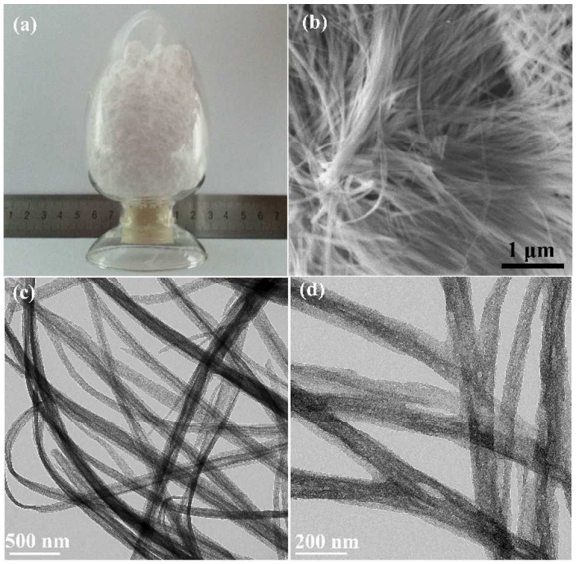

Fig. 2. (a) Photographic image of the product. (b) Typical SEM images of the porous BN nanofibers (pyrolysis treated at 1100 °C). (c) TEM image showing flexible nanofibers with a high aspect ratio. (d) Enlarged TEM image of the product, revealing the porous nanofiber structure.

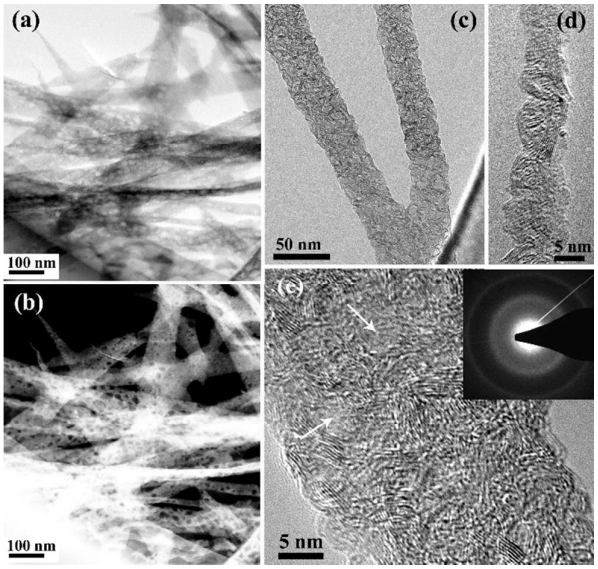

Fig. 3. (a, b) Bright-field STEM image and the corresponding HAADF STAM image of the nanofibers (pyrolysis treated at 1100 °C), respectively, clearly displaying the porous nature of nanofibers. (c) Representative TEM images of individual nanofibers. (d) TEM image of a single nanofiber with downsized diameter of sub-10 nm. (e) HRTEM image indicating the formation of pores in the nanofiber. (inset) The corresponding SAED pattern.

Journal Name

ARTICLE

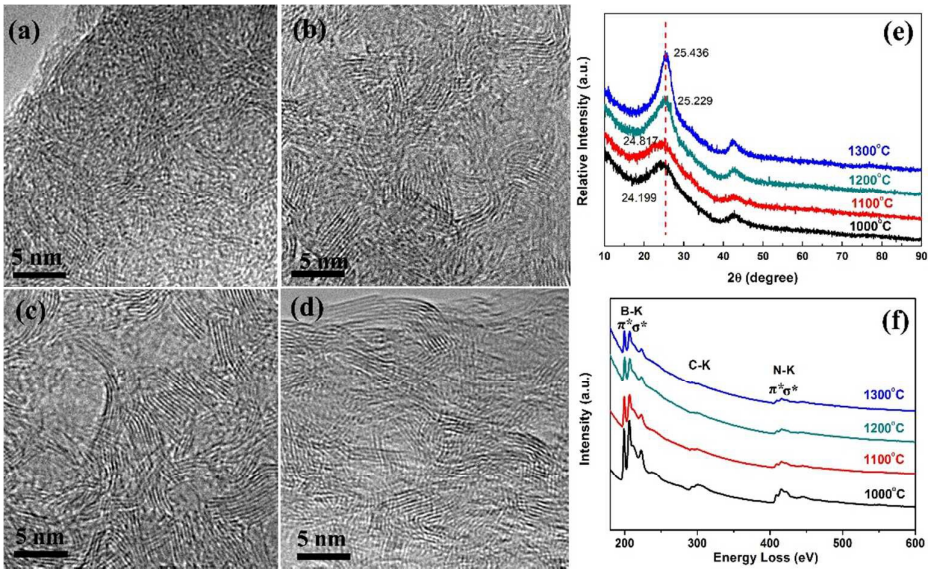

Fig. 4. (a-d) HRTEM image of porous BN nanofibers prepared at different pyrolysis temperatures: (a) 1000°C; (b) 1100°C; (c) 1200°C; (d) 1300°C. XRD patterns (e) and EELS profile (f) of the nanofibers prepared at different pyrolysis temperatures.

observed, reflecting the lattice distance decreases from 0.376 nm (nanofibers obtained at 1000°C) to 0.359 nm (nanofibers obtained at 1300°C). Fig. 4f presents the EELS profiles of as-synthesized BN nanofibers. All spectra show the intense B and N K-edges, respectively. The π* peaks (as marked) for B and N is a characteristic of the sp2 bonding configuration. Quantitative analysis confirms that the BN nanofibers mainly consist of B and N with a small amount of C and O. With increasing the pyrolysis temperature, the contents of C and O tend to decrease. The main composition of BN nanofibers prepared at 1300°C is B and N with a molar ratio of ca. 1.0 , and a very small content of C (~2 at %) and O (< 0.1 at %).

Then the specific surface areas and porosity of all pyrolysis treated products are investigated using N_2 adsorption and desorption isotherms measured at 77 K, and the results are shown in Fig. 5a. As can be seen, a typical N_2 adsorption/desorption isotherm of BN nanofibers synthesized at 1100°C can be classified as type IV isotherm based on the IUPAC classification, and exhibits a H4 type hysteresis loop. In particular, the measured isotherm shows a rapid increase of N_2 adsorptions at relative low pressure range, implying the presence of micropores in the nanofibers. Besides, the H4 hysteresis loop indicates that the BN nanofibers contain narrow slit-shaped mesopores. As the relative pressure increases to ~1 ($P/P_0 \approx 1$), a great enhancement of N_2 adsorptions can be observed, indicating the existence of macrospores in the product. We anticipate that the macrospores can be attributed to the accumulation of numerous nanofibers, which is in an excellent agreement with our SEM and low-magnification TEM observations. The isotherms for nanofibers obtained at 1000, 1200 and 1300°C display similar results. The BET specific surface areas of all the samples were calculated using a multipoint BET method, and the results are summarized in Fig. 5b. Compared with BN nanofibers obtained at other temperatures, the 1100°C-annealed sample displays a much higher specific surface area of 515 m^2/g and a high pore volume of 0.566 cm^3/g. To understand this phenomenon, we calculated the pore size distribution (PSD) using a non-local density functional theory (NLDFT) method.[27,28] As shown in Fig. 5c, the BN nanofibers have a broad PSD with the main characteristic pore size of ~1.4 nm, ~1.7 nm and ~2.7 nm. In particular, the 1100°C-annealed BN sample has the largest micropore volume (as shown in Fig. 5b). Combined with the HRTEM and XRD results, we can conclude that the decrease of specific area and pore volume for high-temperature-samples (above 1100°C) can be attributed to the ordering or crystallization of layered BN materials at very high temperatures.

In order to further clarify the growth mechanism of the nanofibers, we synthesized porous BN without using the freeze-drying process for comparison. In detail, a naturally cooling process of hot $H_3BO_3/C_3N_6H_6$ solution was utilized instead of the liquid nitrogen freeze-drying treatment. The

final product consists of BN whiskers with diameters of 5-10 μm (Fig. S2,

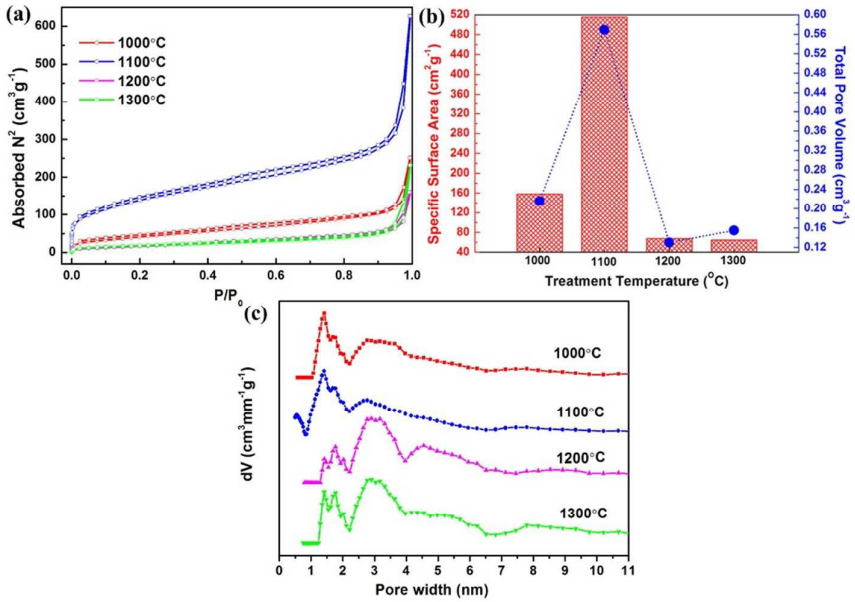

Fig. 5. (a) Nitrogen adsorption-desorption isotherms of porous BN nanofibers prepared at different temperatures (1000-1300°C). (b) The summary of BET specific surface areas and total pore volumes of the different samples. (c) The corresponding pore size distributions of the samples derived by using NLDFT method.

Supporting Information). This indicates that the freeze-drying process is the key factor for the ultrafine nanofiber formation. Based on the structural analysis and the synthesis approach, the growth mechanism of porous BN nanofibers can be clarified. Firstly, ultrafine M·2B nanofibers were synthesized by freeze-drying of hot aqueous solution of H_3BO_3 and $C_3N_6H_6$ via the reaction: $2H_3BO_3 + C_3N_6H_6 \rightarrow C_3N_6H_6{\cdot}2H_3BO_3$. The M·2B precursor was a hydrogen-bonded structure consisting of inter-linked planar triangular H_3BO_3 and $C_3N_6H_6$ molecules.[19] Here the M·2B precursors were made by cryodesiccation from the hot aqueous solutions of H_3BO_3 and $C_3N_6H_6$, which was quite different from the natural cooling and precipitate drying process for porous BN whiskers.[19] The liquid nitrogen freezing of hot H_3BO_3 and $C_3N_6H_6$ solution led to a rapid precipitation of numerous M·2B nuclei. Then the M·2B nuclei continuously absorbed newly generated M·2B precipitates to form 1D M·2B nanofibers. The newly formed M·2B nanofibers were frozen in a very short period of time during the extremely rapid cooling process, rather than continuously grow up to micrometer sized whiskers (Fig. S2, Supporting Information). Then the M·2B nanofibers with hydrogen-bonded layered structure were changed into BN nanofibers by the high temperature pyrolysis treatment. It should be noted that, the specific surface area and pore volume of the samples depended on the pyrolysis temperature. There were two processes taking place during the annealing of precursors at around 1100°C. One was the release of gaseous groups, such as H_2O, NH_3, N_2 and CO from the M·2B precursors. Another was the crystallization process of the left BN. When the annealing temperature was lower or equal to 1100°C, the former process was dominated and led to the increase of the number of porosities and specific surface area. When the temperature was above 1100°C, the crystallization of BN began to speed up. The ordering of layered BN led to merging of the micropores and as a result, the total pore volumes shrunk and the specific surface areas decreased.

Due to their porous nature with high specific surface area, we anticipate that our porous BN nanofibers can be valuable adsorbent for wastewater treatment. Accordingly, we investigate the adsorption performance of our porous BN nanofibers for the removal of MB, one of the commonly used cationic dyes in the textile industry. After adding 50 mg of porous BN nanofibers (pyrolysis treated at 1100°C) into 200 ml of MB solution with an initial concentration of 20 mg/L, the UV-Vis spectra of the MB solution collected at different time intervals are shown in Fig. 6a. Fig. 6b shows the corresponding adsorption rate curve. As can be seen, ~97.6% of MB was removed from the solution within 2 min of reaction, indicating a rapid adsorption capability of our BN nanofibers. Inset of Fig. 6b shows adsorption rate curves of BN nanofibers for the removal of MB with different concentrations. Although the

Journal Name

ARTICLE

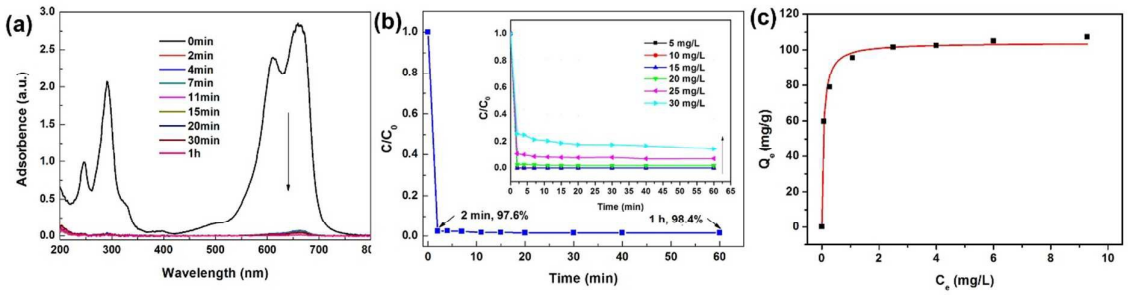

Fig. 6. (a) UV-Vis absorption spectra of the MB solution (20 mg/L, 200 ml) at different time intervals after adding 50 mg porous BN nanofibers (pyrolysis treated at 1100°C). (b) The corresponding adsorption rate curve. (inset) Adsorption rate curves of MB on BN nanofibers with different solution concentrations. (c) Adsorption isotherms of MB on porous BN nanofibers.

removal of MB decreases with increasing in initial MB concentration, all of the adsorption equilibrium may be achieved in a very short time (almost within ~2 min), indicating an ultrafast removal rate of the porous BN nanofibers. Fig. 6c shows the adsorption isotherm of MB on the porous BN nanofibers. The experimental data fit the Langmuir model[29] well, with the correction coefficient of 0.989, corresponding to complete monolayer covering of the adsorbent (also see Fig. S3 and Table 1, Supporting Information). The maximum adsorption capacity of porous BN nanofibers for MB is 107.3 mg/g. The as-prepared porous BN nanofibers display an ultrafast adsorption rate compared with many reported adsorbents, such as grapheme oxide nanosheets,[30] MnO_2 hollow nanostructures,[31] NiO nanosheets,[32] porous BN nanosheets,[16] and BN hollow spheres.[17] The fast adsorption rate can be attributed to the large external surface of the ultrafine 1D nanostructures, the high specific surface areas, and negatively charged BN surfaces.[33] When porous BN crystallized in 1D nanostructure, a large amount of micropores tend to distribute on the external surface of the 1D nanofibers,[34] resulting in a large number of adsorption sites for dye molecules. So the porous BN nanofibers show a faster diffusion rate compared with bulk or micrometer-sized porous materials. Besides, the strong electrostatic interaction between the cationic dye molecules to the external surfaces of negatively charged BN is also beneficial for their adsorption performances.[18] Moreover, we believe that the unique 1D nanostructure with high aspect ratio is also a great advantage for the further assembly of the porous BN nanofibers into filtration membrane for their practical adsorbent applications. We have also studied the adsorption performances of porous BN nanofibers for another kind of dye, i.e. Rhodamine B (RhB). Similarly, an ultrafast adsorption rate was observed (Fig. S4, Supporting Information). Therefore, the present porous BN nanofibers can be considered as valuable adsorbent for highly efficient remove of hazardous dyes.

Conclusions

In summary, we have successfully synthesized ultrafine porous BN nanofibers via a green, two-step, template-free method. Firstly, a freeze-drying process was developed to obtain ultrafine M·2B nanofibers as a precursor. After a high temperature pyrolysis treatment, ultrafine porous BN nanofibers in a high yield and high purity were finally obtained. The extremely rapid cooling of hot melamine and boric acid solutions during the cryodesiccation process is the key factor for the formation of BN nanofibers with downsized diameters. The product consists of pure nanofibers with diameters of 20-60 nm and lengths of tens micrometers. A moderate pyrolysis temperature results in the production of porous BN nanofibers with a high specific surface area of 515 m^2/g, a total pore volume of 0.566 cm^3/g, and a broad PSD with main characteristic pore size of ~1.4 nm, ~1.7 nm and ~2.7 nm. The porous BN nanofibers show highly efficient MB removal performances with an ultrafast adsorption rate. The present novel porous 1D nanostructures are envisaged to show high potentials in prospective applications including wastewater treatment, reinforcing agents for functional composites, catalyst carrier, etc.

Acknowledgements

This study was supported by the National Natural Science Foundation of China (51332005, 51372066, 51202055, 51402086, 51572068), the Australian Research Council, the Program for Changjiang Scholars and Innovative Research Team in University (PCSIRT: IRT13060), the Hundred Talents

Program of Hebei Province (E2014100011), and the Tianjin Research Program of Application Foundation and Advanced Technology (14JCYBJC42200). The Australian Microscopy & Microanalysis Research Facility is gratefully acknowledged for providing access to the facilities used in this work.

Notes and references

1 T. Zhai, L. Li, Y. Ma, M. Liao, X. Wang, X. Fang, J. Yao, Y. Bando and D. Golberg, *Chem. Soc. Rev.* 2011, **40**, 2986.
2 R. S. Devan, R. A. Patil, J. H. Lin and Y. R. Ma, *Adv. Funct. Mater.* 2012, **22**, 3326.
3 Z. G. Chen, J. Zou, G. Liu, F. Li, Y. Wang, L. Wang, X. L. Yuan, T. Sekiguchi, H. M. Cheng and G. Q. Lu, *ACS Nano*, 2008, **2**, 2183.
4 X. Fang, Y. Bando, U. K. Gautam, T. Zhai, S. Gradecak and D. Golberg, *J. Mater. Chem.* 2009, **19**, 5683.
5 R. Arenal and A. Lopez-Bezanilla, Wiley Interdisciplinary Reviews: Computational Molecular Science, 2015, **5**, 299.
6 Y. Huang, Y. Bando, C. Tang, C. Zhi, T. Terao, B. Dierre, T. Sekiguchi and D. Golberg, *Nanotechnology*, 2009, **20**, 085705.
7 D. Golberg, Y. Bando, Y. Huang, T. Terao, M. Mitome, C. Tang and C. Zhi, *ACS Nano*, 2010, **4**, 2979.
8 D. Golberg, Y. Bando, C. Tang and C. Zhi, *Adv. Mater.*, 2007, **19**, 2413.
9 C. Y. Zhi, Y. Bando, C. C. Tang, Q. Huang and D. Golberg, *J. Mater. Chem.*, 2008, **18**, 3900.
10 C. H. Lee, M. Xie, Y. Kayastha, J. Wang and Y. K. Yap, *Chem. Mater.*, 2010, **22**, 1782.
11 L. H. Li, Y. Chen and A. M. Glushenkov, *Nanotechnology*, 2010, **21**, 105601.
12 Y. Huang, J. Lin, C. Tang, Y. Bando, C. Zhi, T. Zhai, B. Dierre, T. Sekiguchi and D. Golberg, *Nanotechnology*, 2011, **22**, 145602.
13 W. Q. Han, R. Brutchey, T. D. Tilley, A. Zettl, *Nano Lett.*, 2004, **4**, 173.
14 A. Vinu, M. Terrones, D. Golberg, S. Hishita, K. Ariga and T. Mori, *Chem. Mater.*, 2005, **17**, 5887.
15 S. Schlienger, J. Alauzun, F. Michaux, L. Vidal, J. Parmentier, C. Bervais, F. Babonneau, S. Bernard, P. Miele and J. B. Parra, *Chem. Mater.*, 2012, **24**, 88.
16 W. Lei, D. Portehault, D. Liu, S. Qin and Y. Chen, *Nat. Commun.*, 2013, **4**, 1777.
17 G. Lian, X. Zhang, S. Zhang, D. Liu, D. Cui and Q. Wang, *Energy Environ. Sci.*, 2012, **5**, 7072.
18 G. Lian, X. Zhang, H. Si, J. Wang, D. Cui and Q. Wang, *ACS Appl. Mater. Interfaces*, 2013, **5**, 12773.
19 J. Li, J. Lin, X. Xu, X. Zhang, Y. Xue, J. Mi, Z. Mo, Y. Fan, L. Hu, X. Yang, J. Zhang, F. Meng, S. Yuan and C. Tang, *Nanotechnology*, 2013, **24**, 155603.
20 J. Li, X. Xiao, X. Xu, J. Lin, Y. Huang, Y. Xue, P. Jin, J. Zou and C. Tang, *Sci. Rep.*, 2013, **3**, 3208.
21 Q. Weng, X. Wang, Y. Bando and D. Golberg, *Adv. Energy Mater.*, 2014, **4**, 1301525.
22 Q. Weng, X. Wang, C. Zhi, Y. Bando and D. Golberg, *ACS Nano*, 2013, **7**, 1558.
23 C. C. Tang, Y. Bando, X. X. Ding, S. R. Qi and D. Golberg, *J. Am. Chem. Soc.*, 2002, **124**, 14550.
24 H. Zhang, C. J. Tong, Y. Zhang, Y. N. Zhang and L. M. Liu, *J. Mater. Chem. A* 2015, **3**, 9632.
25 M. Maleki, A. Beitohhahi and M. Shokouhimehr, *Eur. J. Inorg. Chem.*, 2015, 2478.
26 X. Zhang, G. Lian, H. Si, J. Wang, D. Cui and Q. Wang, *J. Mater. Chem. A* 2013, **1**, 11992.
27 P. Tarazona, U. M. B. Marconi and R. Evans, *Mol. Phys.* 1987, **60**, 573.
28 M. L. Occelli, J. P. Olivier, A. Petre and A. Auroux, *J. Phys. Chem. B* 2003, **107**, 4128.
29 M. X. Zhu, L. Lee, H. H. Wang and Z. Wang, *J. Hazard. Mater.* 2007, **149**, 735.
30 H. Guo, T. Jiao, Q. Zhang, W. Guo, Q. Peng and X. Yan, *Nanoscale Res. Lett.* 2015, **10**, 272.
31 J. Fei, Y. Cui, X. Yan, W. Qi, Y. Yang, K. Wang, Q. He and J. Li, *Adv. Mater.* 2008, **20**, 452.
32 B. Cheng, Y. Le, W. Cai and J. Yu, *J. Hazard. Mater.* 2011, **185**, 889.
33 J. Li, Y. Huang, Z. Liu, J. Zhang, X. Liu, H. Luo,Y. Ma, X. Xu, Y. Lu, J. Lin, J. Zou and C. Tang, *J. Mater. Chem. A* 2015, **3**, 8185.
34 S. Mintova, J. P. Gilson and V. Valtchev, *Nanoscale* 2013, **5**, 6693.